

Interface magnetism and electronic structure: ZnO(0001)/Co₃O₄(111)I.M. Kupchak,¹ N.F. Serpak,¹ A. Chkrebti,² and R. Hayn³¹*V.Lashkarev Institute of semiconductor physics, NAS Ukraine, 45, pr.Nauky, Kyiv, 03680, Ukraine* ^{a)}²*Institute technology of University of Ontario, 2000 Simcoe Street North Oshawa, Ontario L1H 7K4 Canada*³*Aix-Marseille Univ., CNRS, IM2NP-UMR 7334, 13397 Marseille Cedex 20, France*

We have studied the structural, electronic and magnetic properties of spinel Co₃O₄ (111) surface and its interface with ZnO (0001) using density functional theory (DFT) at the Generalized Gradient Approximation with on-site Coulomb repulsion term (GGA+U). Two possible forms of spinel surface, containing Co²⁺ and Co³⁺ ions and terminated with either cobalt or oxygen ions were considered, as well as their interface with zinc oxide. Our calculations shows that Co³⁺ ions have non-zero magnetic moments at the surface and interface, in contrast to the bulk where they are not magnetic, leading to the ferromagnetic ordering. Since some heavily Co-doped ZnO samples may contain Co₃O₄ secondary phase, such a magnetic ordering might be the possible origin of the magnetism.

PACS numbers: 73.20.-r, 75.70.-i

^{a)}Electronic mail: Electronic address: kupchak@isp.kiev.ua

CONTENTS

I. Introduction	2
II. Numerical Method	5
III. Surface and interface structural details	6
IV. Results and discussion	8
V. Conclusion	12
Acknowledgments	12
References	13

I. INTRODUCTION

Magnetic semiconductors (MS) and diluted magnetic semiconductors (DMS) exhibit both ferromagnetic and semiconducting properties and are interesting materials for spintronics using not only the electron charge but also its spin for information processing. Historically, the first DMS with a high Curie temperature up to about 200 K was GaAs doped with Mn ions^{23,30}. In that compound, the ferromagnetism is promoted by hole carriers which align the local Mn moments (carrier-induced ferromagnetism or Zener $p - d$ exchange). It is essential for that mechanism that Mn at the Ga site becomes Mn^{2+} instead of Ga^{3+} providing at the same time a local spin and a hole charge carrier. In a very influential paper⁸ Dietl and co-workers predicted above room-temperature ferromagnetism in $\text{ZnO}:\text{Co}$ and $\text{GaN}:\text{Mn}$ provided the same carrier-induced mechanism would be at work with a sufficiently high number of hole charge carriers. First experiments after that prediction seemed to confirm the proposal¹⁹ being supported by *ab-initio* calculations³⁹ but it soon turned out that the Co impurity is in fact isovalent to the Zn ion³⁸ and provides no charge carriers at all. The situation in $\text{GaN}:\text{Mn}$ is similar⁴² but we are going to concentrate here on $\text{ZnO}:\text{Co}$. Nevertheless, experimental reports on above room-temperature ferromagnetism in $\text{ZnO}:\text{Co}$ persist whose mechanism is not clarified up to now. There exist several attempts to explain the mechanism of ferromagnetism in realistic $\text{ZnO}:\text{Co}$ systems reaching from

spinodal decomposition⁹ up to Lieb-Mattis ferrimagnetism¹⁸ to cite just two ideas.

The typical doping level of Co in ZnO can be relatively high (in the range between 10% and 30%), leading to secondary phases of Co_3O_4 and ZnCo_2O_4 segregation during the sample growth, which can be detected, for instance, by Raman spectroscopy^{7,48}. Although, in general, the appearance of such secondary phases is detrimental for the DMS materials, this effect can also be advantageous. It can eventually provide one of the possible explanations in the big puzzle of the nature of ferromagnetism in DMS, but it is also promising for new applications. However, a lack of understanding of the secondary phases and their interfaces remains currently the main obstacle toward the practical applications of Co_3O_4 surfaces and interfaces.

Cobalt oxide Co_3O_4 (also known as tricobalt tetraoxide or cobalt spinel) is a *p*-type semiconductor with the reported optical energy gap E_g between 1.1 and 1.65 eV (see⁴⁶ and ref. therein). It is widely used in lithium-ion batteries as a cathode material⁴¹, gas sensing, nano-materials and nano-junctions, environmental and various other applications^{1,16,26,28}. Co_3O_4 crystallizes in the cubic normal spinel structure, which contains cobalt ions in two different oxidation states, Co^{2+} and Co^{3+} , located at the interstitial tetrahedral (A) and octahedral (B) sites, respectively (see., *e.g.*, Ref.⁴⁶). In the presence of tetrahedral crystal field, five-fold degenerate atomic *d* orbitals of Co^{2+} ions are split into two groups, e_g and t_{2g} , leading to three unpaired *d* electrons on t_{2g} orbital. Similarly, in a case of Co^{3+} , the crystal field is octahedral, and the splitting leads to six paired electrons in the t_{2g} orbital, while e_g orbital is empty. As a result, the Co^{2+} ions carry a permanent magnetic moment, whereas Co^{3+} ions are not magnetic. Considering the A-site sublattice only, each Co^{2+} ion is surrounded by four neighbors with oppositely directed spin, thus forming an antiferromagnetic state. In general, such nearest A-A exchange interaction is expected to be weak, since in typical spinel structures with magnetic cations A-B coupling between the ions in tetrahedral and octahedral sites is dominant³⁷. However, in the Co_3O_4 spinel this A-A coupling is unusually strong due to the indirect exchange through the intermediate Co^{3+} ions in the octahedral B-site, providing Co^{2+} ions by a magnetic moment of about $3.02 \mu_B$. As a result of such strong coupling, Co_3O_4 is antiferromagnetic below the Neel temperature $T_N \sim 40 \text{ K}$ and paramagnetic at higher temperatures³⁷.

When such a complex structure is terminated by a surface or forms an interface, one can expect new interesting magnetic peculiarities, absent in the bulk of the crystal. Indeed,

the formation of surface or interface between different materials involves several important factors such as, *e.g.*, surface polarity, charge transfer, stresses, defects, *etc.*, altering the long-range magnetic ordering, and the magnetic response as a result^{29,36}. There are many publications on the electron and magnetic properties of different spinels and their surfaces, such as Fe_3O_4 spinel (see, *e.g.*,²⁹), which has the crystal structure similar to that of Co_3O_4 . However, the cobalt spinel surfaces are still not that well understood, while even more complex behaviour should be expected when the interface with other materials is formed. It has been shown that during the epitaxial growth of Co_3O_4 , two surfaces with the lowest surface energy, namely (111) and (110), are typically formed¹⁴. More detailed experimental and theoretical study have been performed in⁴³, where the effect of different Co_3O_4 crystal planes orientation on reducing charge-discharge over-potential toward an application in high energy density Li – O_2 batteries has been investigated and established, that (111) plane is the most efficient. Experimentally, cobalt spinel (110) surface was thoroughly investigated by Petitto and Langel³⁴ using low energy electron diffraction (LEED), Auger electron spectroscopy (AES), and x-ray photoelectron spectroscopy (XPS). The Co_3O_4 (111) surface has been studied by X-ray diffraction (XRD) and atomic force microscopy (AFM) methods⁴, LEED and scanning tunneling microscopy (STM)^{10,24,44,45}. Bulk Co_3O_4 have also been studied using Raman spectroscopy¹³. In general, Co_3O_4 attracts the interest because of its high catalytic activity, especially for CO oxidation, therefore most of the research have been performed toward such an application. Concerning the theory, a number of publications has been dedicated to *ab-initio* study of electronic and magnetic properties of the bulk and surfaces of Co_3O_4 ^{5,6,27,40,47,49,51}. The main problem, discussed in the above cited theoretical works, was usually a nature of superexchange in bulk spinel and the stability of its surfaces under different conditions, such as different atom types (Co^{2+} , Co^{3+} ions, or O) at the top layer termination.

Another field of cobalt spinel application is related to the interface between *p*-type Co_3O_4 and *n*-type ZnO, which forms *p-n* heterojunction. In particular, *p* – Co_3O_4 /*n* – ZnO composites can provide higher sensitivities and faster responses toward gas sensing application^{2,15,26,32,50}. Such composites are typically obtained using a mixture of ZnO and Co_3O_4 powders and following annealing, that forms inhomogeneous interface between both semiconductors. However, the presence of this interface also plays a significant role in the magnetic properties of such composites. Indeed, there is an evidence of the magnetism

appearance in ZnO/Co₃O₄ powder mixture at room temperature even without thermal treatment^{21,35}. Authors explain this phenomena by surface reduction of the Co₃O₄ nanoparticles, in which the antiferromagnetic Co₃O₄ nanoparticle is surrounded by a CoO-like shell. Other authors^{11,22}, studying ZnO/Co₃O₄ powder mixture by X-ray absorption spectroscopy (XAS) and optical spectroscopy, explained such phenomena by reduction $\text{Co}^{3+} \rightarrow \text{Co}^{2+}$ at the Co₃O₄ particle surface. This explanation has been proved by Vibrating Sample Magnetometer (VSM) analysis of composite ZnO synthesized on the surface of core Co₃O₄ in¹⁷. Recently a diode consisting of *p*-type Co₃O₄ nanoplate / *n*-type ZnO nanorods heteroepitaxial junction has been fabricated, showing reasonable electrical performance²⁰, but no attention has been paid to its magnetic properties.

Considering a lack of the microscopic understanding of the interface magnetism, the present study is aimed to establish the nature of ferromagnetism at the Co₃O₄/ZnO interface toward an application in the new type devices for spintronics. We have investigated from the first principles modification of the atomic structure at various types of the Co₃O₄/ZnO boundaries, related changes in the electron band structure and their contribution to the appearance of the interface magnetic properties. The paper is organized as following. We present in Section 2 the numerical formalism which is used throughout the paper. Section 3 discusses the microscopic atomic structure of the surfaces and interfaces under consideration. The results of the calculated magnetic and electronic properties and their modifications due to the surfaces or interfaces, are discussed in Section 4. The conclusion is presented in Section 5.

II. NUMERICAL METHOD

The atomic and electronic structure of the Co₃O₄/ZnO interface was investigated within the density functional theory (DFT) and generalized gradient approximation (GGA), as implemented in the Quantum-Espresso software package¹². We have used ultrasoft Perdew-Burke-Ernzerhof pseudopotentials³³ which include 12 valence electrons for zinc, 6 valence electrons for oxygen, and 9 valence electrons for cobalt. An integration of the Brillouin zone has been performed using 4×4 Γ -centered grid of special points in *k*-space, generated by Monkhorst-Pack scheme³¹ and Methfessel-Paxton smearing²⁵ with a parameter of 0.005 Ry. Several tests were performed with denser grids up to 10×10 , but no significant changes

have been observed compared to the case of 4×4 grid. To ensure a sufficient convergence of the results we applied 40 Ry cutoff for smooth part of the wave function and 400 Ry for the augmented charge density. We approximated the exchange-correlation functional with both the local spin resolved generalized gradient approximation (SGGA) and the so-called SGGA+U approximation, in which the effect of electron correlations in the $3d$ shell is taken into account by considering the on-site Coulomb interactions within the Hubbard method. We have chosen the value of Hubbard U parameters to be 3.5 eV and 5.0 eV for Co and Zn atoms, respectively. Although these values of Hubbard parameters are commonly accepted in the literature, they still are the subject of discussion⁴⁰. But we have checked that our conclusions do not depend in a sensitive way on these Coulomb parameters. Throughout our study we have performed the structural relaxations with the SGGA method but the final calculations of the magnetic structure and the densities of states by the SGGA+U method. The systems were relaxed through all the internal coordinates until the Hellmann-Feynman forces became less than 10^{-4} a.u., while keeping the shape and volume of the supercell fixed.

III. SURFACE AND INTERFACE STRUCTURAL DETAILS

The bulk terminated atomic structure of Co_3O_4 (111) spinel surface in $[111]$ direction, perpendicular to the surface, can be described by a sequence of atomic layers, containing Co^{2+} ions or both of Co^{2+} and Co^{3+} ions, separated by layer of oxygen: $\text{O} - \text{Co}^{2+} - \text{O} - \text{Co}^{2+}\text{Co}^{3+}$. The primitive unit cell, containing such a sequence, has a hexagonal symmetry along the surface or the interface. The top layer, which forms the interface with ZnO, contains either three Co^{3+} ions (B-terminated layer) or a combination of two Co^{2+} and one Co^{3+} ions (A-terminated layer, since the closest to the interface cobalt oxide layer is of A-type). The interface between the top layer of Co_3O_4 and ZnO is then being formed by introducing a single layer of four oxygen atoms to match the CoO bonds of a spinel. These four oxygen atoms can also be viewed as those belonging to ZnO in a sequence $\text{Zn}-\text{O}-\text{Zn}-\text{O}$ of the primitive unit cell: the topology of this spinel oxygen layer has the same symmetry as (0001) plane of hexagonal ZnO. Hence, to form the epitaxial interface with Co_3O_4 , four primitive unit cells of hexagonal ZnO are required to saturate these oxygen bonds. In such a way, oxygen atoms play a role of a bridge between cubic spinel Co_3O_4 and wurtzite ZnO.

Considering the experimental value of bulk spinel lattice constant $a_{\text{spinel}} = 8.084 \text{ \AA}$, prim-

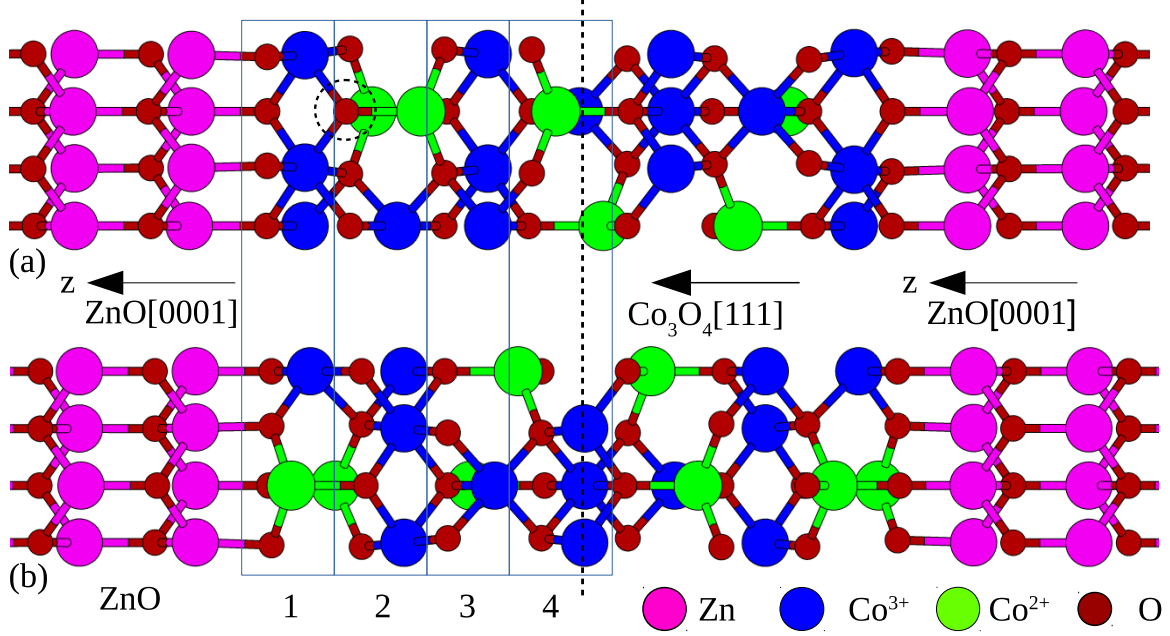


FIG. 1. (Color online) Side view of unit cells of Co₃O₄/ZnO interfaces: (a) Octahedral B-terminated interface, (b) Tetrahedral A-terminated interface. Numbers denote the atomic layers of both interfaces.

itive unit cell of its (111) surface has a lattice constant $c_{spinel} = 5.72 \text{ \AA}$, while a corresponding parameter of ZnO has a value $c_{ZnO} = 3.25 \text{ \AA}$. In order to fit four primitive unit cells of ZnO onto single 2D unit cell of spinel, the bulk constant of ZnO should be compressed in the basal plane by about 12%. Therefore, the lattice constant of this strained ZnO at the interface region is 2.86 \AA . As it has been suggested in²⁰, such a large stress is relieved by forming dislocations along basal plane at the interface. Additionally, due to low-sized diameters of the segregated phase regions, the strain can be accommodated through the lateral relaxation, allowing the heteroepitaxy, even in the case of such high lattice mismatch³. In the present calculations such a stress effect is partially taken into account by the system relaxation within the unit cell. The study of extended dislocations forming requires the use of significantly larger unit cells and therefore lays out of our model.

To study magnetic and electronic structures of an interface, we built two symmetric slabs, containing five atomic layers of Co₃O₄, and adjacent on both sides ZnO layers, as shown in Fig. 1. The first slab (Fig. 1a) is composed of spinel top layer containing Co³⁺ ions only (octahedral interface), while the second slab (Fig. 1b) is created using atomic layer,

containing both Co^{2+} and one Co^{3+} ions (tetrahedral interface). In such a way, each slab contains two interface regions of the same symmetry (topology), so their total dipole moment is close to zero. The ZnO slab is two lattice constants c_{ZnO} thick on both sides and 12 Å of vacuum layer have been added to separate the slabs in z direction. Such a thick slab is necessary because in the systems with ZnO layer of only one lattice constants c_{ZnO} , both spinel and ZnO layers, which form the interface, do not keep adequate crystal structure during the relaxation. Additionally, we have studied the properties of the bulk spinel, using the $12 \times 12 \times 12$ k -point grid, and its clean (111) surface within the same method, described above. We simulated the Co-terminated and O-terminated spinel (111) surfaces using the slabs for the interface model, but with ZnO layers removed and subsequent relaxation over all coordinates.

IV. RESULTS AND DISCUSSION

The calculated lattice constant for bulk spinel $a_{\text{spinel}} = 8.147$ Å, and the corresponding interplanar A-B spacing $d_{111} = 2.351$ Å are overestimated by 0.8% compared to the experimental values of $a_{\text{spinel}} = 8.084$ Å and $d_{111} = 2.333$ Å, respectively.

As mentioned in Sec.3, the unit cell of the spinel (111) plane in the slab construction is hexagonal, and therefore 4 unit cells of ZnO (also hexagonal) are needed to match 1 spinel unit cell. Consequently, the planar lattice constant $a_{\text{ZnO}} = 2.88$ Å must be half of the planar spinel lattice constant and cannot be optimized. Or in other words, the ZnO lattice constant is scaled to the spinel lattice constant. However, the interplanar distances (in z direction) are optimized, for both the spinel and the wurtzite regions of the interface. Therefore, the calculated value of the interplanar spacing at the spinel region of the interface becomes $d_{111} = 2.387$ Å, which is about 2% larger than the experimental bulk interplanar distance, while the lattice constant, calculated for ZnO regions, $c_{\text{ZnO}} = 5.52$ Å, which is about 5% above the corresponding experimental bulk value 5.27 Å. These relaxations absorb part of the stress due to the lattice mismatch between spinel and wurtzite. The optimized supercells of $\text{Co}_3\text{O}_4/\text{ZnO}$ interfaces are depicted on Fig. 1. Since there are no dangling bonds at the interfaces and all the ions are located in such a way that the bulk crystalline symmetry is preserved, no significant modifications in a topology of adjacent atomic layers were found during the relaxation. In the case of surfaces, B-terminated sample demonstrates a top layer

reordering: oxygen atom of layer 2 (O atom circled by dashed line in Fig. 1a) moves toward z -direction occupying the position in-plane with Co atoms of layer 1. Such reordering occurs in Co^{3+} -terminated surface only: A-terminated surfaces with both Co and O top layers and B-terminated with O top layer demonstrate stable surface topology with no significant changes. We have also performed geometry optimization for 9 atomic layers thick Co_3O_4 slabs, and found that the results are practically identical to the case, considered in Fig. 1.

TABLE I. Largest magnetic moments (in the units of μ_B) of Co ions, calculated using Löwdin charge analysis for octahedral surfaces and interfaces

	Co-terminated surface	O-terminated surface	ZnO-interface	Bulk
Co^{3+}	2.33	0.71	0.21	0.0
Co^{2+}	2.45	2.48	2.46	2.59

It has been discussed above that in bulk spinel Co^{3+} ions are non-magnetic due to large splitting between t_{2g} and e_g orbitals, caused by the presence of octahedral crystal field. Since this symmetry is broken at the surface or interface, the electrons could occupy t_{2g} and e_g orbitals in different order, leading to the changes in magnetic properties, as reported in^{5,11}. To quantify these changes, we calculated and compared the magnetic moment of Co ions for different interface and surface systems using a Löwdin charge analysis. Table 1 shows the largest values of magnetic moments, calculated for the bulk Co_3O_4 , interfaces and surfaces, both Co- and O-terminated. The magnetic moments for Co^{3+} ions are calculated for the top layer and for Co^{2+} ions in the second layer of octahedral interface or surface. The deviation of the magnetic moment of the same ion type on different sites is relatively small $\sim 0.02 \mu_B$ for all of systems, so such values are reflecting the general physical picture.

Calculated magnetic moment of Co^{2+} ions in bulk spinel is $2.59 \mu_B$ and becomes slightly smaller in the case of surfaces, as it is seen from Table I. Instead, while the magnetic moment of Co^{3+} ions is zero in the bulk, it is non-vanishing in the case of the surface. The largest magnetic moment of $2.33 \mu_B$ occurs at the Co-terminated surface, where the bulk symmetry is broken and ion coordination number is reduced at the most. If the surface is O-terminated, the magnetic moment of Co^{3+} ions reduces to $0.71 \mu_B$, while the external oxygen atoms receive a magnetic moment of $0.34 \mu_B$ due to a strong polarization of p -orbitals. It is worth to note, that such values of the magnetic moments were obtained for

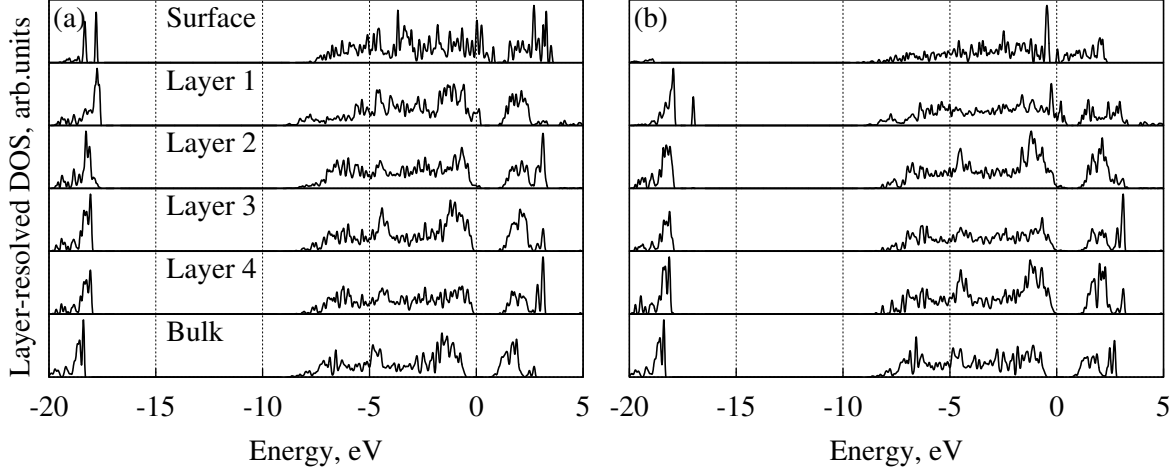


FIG. 2. Layer-resolved DOS of (a) octahedral and (b) tetrahedral spinel (111) surfaces and spinel/wurtzite interfaces. From top to bottom: top layer of spinel (111) surface with no ZnO cap; layers 1 to 4 of the spinel structure close to the spinel/wurtzite interface and the layer-resolved DOS for the (111) plane of bulk spinel (see discussions in the text)

the relaxed systems while keeping the C_{3v} symmetry intact. If this symmetry is broken (for instance, when initial deviations from equilibrium positions are different for symmetry equivalent atoms or due to defects), the corresponding magnetic moments might slightly differ. Nevertheless, the general picture remains the same: Co^{3+} ions are gaining the non-zero magnetic moments both at the surface and interface, in contrast to the bulk case.

As it is generally known, the presence of dangling bonds leads to additional surface states appearing in the density of states (DOS). Formation of the interface between two different materials is responsible for the interface states, localized close to the boundary. The surface or interface formations causes the charge redistribution and change in the corresponding magnetic properties. We calculated the spin-averaged layer-resolved DOS (LRDOS) for all systems under investigation, as shown on the Fig. 2. For bulk spinel, the planes that pass through the Co-ions of corresponding charge state (A or B type) were used as for RLDOS calculations. All LRDOSs there are aligned in such a way that the highest filled states (Fermi level) are at zero energy. For the top layer of Co-terminated surfaces, there is clear evidence of such surface states presence in the DOS (panels on Fig. 2, denoted surface), and such a picture, in principle, is typical for all the considered surfaces with dangling bonds. There is a notable difference in Co-terminated surface DOS for octahedral and tetrahedral termination

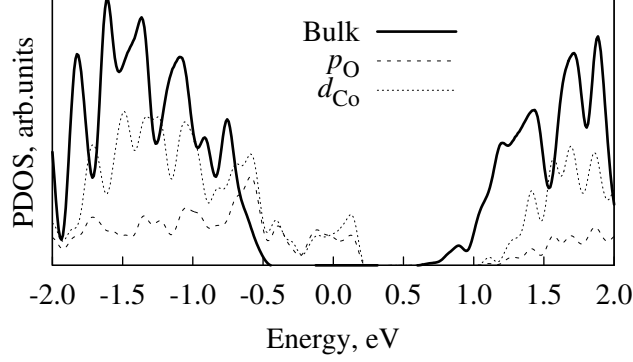


FIG. 3. Projected LRDOS for top layer of octahedral interface and octahedral plane of bulk spinel.

at the region -18 eV, due to the oxygen atom shift from layer 2 and now belonging to the top layer of octahedral system. On the other hand, in tetrahedral system top layer consists of Co atoms only. LRDOS of O-terminated surfaces (not shown) demonstrates no noticeable difference, compared to the Co-terminated surface for both tetrahedral and octahedral coordination. In this case, for both of coordination, the bonds of surface Co atoms now are passivated by oxygen atoms and are not broken anymore. That means, that there are also another factors responsible for the formation of the inside band-gap states. Such a situation is observed also in the case of interface. One can see from Fig. 2 (panels denoted Layer n with $n=1, 2, 3$, and 4), that LRDOS for the first layer demonstrates surface-like states in band-gap close to the top of valence band. For the internal layers these surface-like states are decaying with depth, and finally almost disappearing at Layer 4. Corresponding LRDOS becomes a bulk-like, both for octahedral and tetrahedral coordination, as it is seen from the comparison between LRDOS of Layer 4 and those denoted Bulk on Fig. 2.

Comparing LRDOS calculated for surface and interface, one can conclude, that although each Co-ion at the interface layer keeps the symmetry of the bulk crystalline environment, the physical properties of the interface region is closer to the surface, rather than to the bulk. To study the origin of the surface-like states in the band-gap, we calculated the RLDOS of the octahedral interface, projected onto atomic wavefunctions of corresponding Co atom (s and d orbitals) and O atom (s and p orbitals), localized at the octahedral interface, as shown on Fig. 3. For convenience, we plotted there also LRDOS for A-plane of bulk spinel. As it can be seen, surface-like states originate predominantly from O $2p$ states and Co $3d$ states, while the contribution of s -states of both Co and O is negligibly small here. Similar results

have been also obtained for the origin of the surface states in the tetrahedral systems. From this we conclude that charge state of Co-ion is not decisive in defining the surface or interface magnetism since in both of cases p -orbitals of O-atoms make the same contribution into DOS. Moreover, from the band structure calculation we see that the partially occupied states are common for all of the surfaces and interfaces under investigation. This demonstrates the metal-like electronic structure, in contrast to the bulk spinel, which appears semiconducting in the simulations even when larger smearing parameters in the Brillouin zone integration are used.

V. CONCLUSION

In the present work we investigated the origin of the surface/interface magnetism of the cobalt oxide Co_3O_4 surfaces and its interfaces with zinc oxide ZnO . In particular, we calculated and compared the structural, electronic and magnetic properties of $\text{ZnO}(0001)/\text{Co}_3\text{O}_4$ (111) interfaces, Co_3O_4 (111) surfaces and bulk spinel for A-type and B-type terminations. It is shown, that while the magnetic moment of Co^{3+} ions is zero in the bulk, it does not vanish at the interface or surface, and its value is comparable with the Co^{2+} magnetic moment at the surface. The calculated LRDOS demonstrate, that although Co ions at the interface have the same neighboring atoms as in bulk spinel, they exhibit an interface-like nature of DOS, arising from polarized Co $3d$ and O $2p$ orbitals of the interfacing layer. In all cases, interface or surface, A- or B-type termination, we observe metallic-like states which are localized in the surface or interface and which are responsible for the surface/interface magnetism. Whereas the magnetic order is antiferromagnetic in the insulating bulk spinel at low temperature, the metallic surface/interface states indicate the possibility of a ferromagnetic order in the surfaces or interfaces. That might eventually explain the experimental observation of a net magnetic moment in some Co doped ZnO with high Co concentrations.

ACKNOWLEDGMENTS

The work was supported by Science for Peace and Security Program (the grant NATO NUKR.SFPP 984735). I. Kupchak acknowledges EC for the RISE Project CoExAN GA644076 within HORIZON2020 program. The CPU time was provided by the Shared

REFERENCES

- ¹Bajdich, M., M. García-Mota, A. Vojvodic, J. K. Nørskov, and A. T. Bell (2013), Journal of the American Chemical Society **135** (36), 13521.
- ²Bekermann, D., A. Gasparotto, D. Barreca, C. Maccato, E. Comini, C. Sada, G. Sberveglieri, A. Devi, and R. A. Fischer (2012), ACS Applied Materials & Interfaces **4** (2), 928.
- ³Bekermann, D., A. Gasparotto, D. Barreca, C. Maccato, M. Rossi, R. Matassa, I. Cianchetta, S. Orlanducci, M. Kete, and U. L. Štangar (2012), Crystal Growth & Design **12** (10), 5118.
- ⁴Buršík, J., M. Soroka, R. Kužel, and F. Mika (2015), Journal of Solid State Chemistry **227**, 17.
- ⁵Chen, J., and A. Selloni (2012), Physical Review B **85** (8), 085306.
- ⁶Chen, J., and A. Selloni (2012), The Journal of Physical Chemistry Letters **3** (19), 2808.
- ⁷Dietl, T., T. Andrearczyk, a. Lipińska, M. Kiecana, M. Tay, and Y. Wu (2007), Physical Review B - Condensed Matter and Materials Physics **76** (15), 1, 0708.2476.
- ⁸Dietl, T., H. Ohno, F. Matsukura, J. Cibert, and D. Ferrand (2000), Science **287** (5455), 1019.
- ⁹Dietl, T., K. Sato, T. Fukushima, A. Bonanni, M. Jamet, A. Barski, S. Kuroda, M. Tanaka, P. N. Hai, and H. Katayama-Yoshida (2015), Reviews of Modern Physics **87** (4), 1311.
- ¹⁰Ferstl, P., S. Mehl, M. a. Arman, M. Schuler, a. Toghan, B. Laszlo, Y. Lykhach, O. Brummel, E. Lundgren, J. Knudsen, L. Hammer, M. a. Schneider, and J. Libuda (2015), The Journal of Physical Chemistry C **119** (111), 16688.
- ¹¹García, M. a., F. Jinez-Villacorta, a. Quesada, J. De La Venta, N. Carmona, I. Lorite, J. Llopis, and J. F. Fernández (2010), Journal of Applied Physics **107** (4), 1, 0912.3458.
- ¹²Giannozzi, P., S. Baroni, N. Bonini, M. Calandra, R. Car, C. Cavazzoni, D. Ceresoli, G. L. Chiarotti, M. Cococcioni, I. Dabo, A. D. Corso, S. de Gironcoli, S. Fabris, G. Fratesi, R. Gebauer, U. Gerstmann, C. Gougoussis, A. Kokalj, M. Lazzeri, L. Martin-Samos, N. Marzari, F. Mauri, R. Mazzarello, S. Paolini, A. Pasquarello, L. Paulatto, C. Sbraccia, S. Scandolo, G. Sclauzero, A. P. Seitsonen, A. Smogunov, P. Umari, and R. M. Wentzcovitch (2009), Journal of Physics: Condensed Matter **21** (39), 395502.

- ¹³Hadjiev, V. G., M. N. Iliev, and I. V. Vergilov (1988), Journal of Physics C: Solid State Physics **21** (7), L199.
- ¹⁴Hutchison, J., and N. Briscoe (1985), Ultramicroscopy **18** (1-4), 435.
- ¹⁵Jana, T. K., A. Pal, and K. Chatterjee (2015), Journal of Alloys and Compounds **653**, 338.
- ¹⁶Kim, H.-J., and J.-H. Lee (2014), Sensors and Actuators B: Chemical **192**, 607.
- ¹⁷Kulkarni, S. A., P. Sawadh, and P. K. Palei (2014), Journal of the Korean Chemical Society **58** (1), 100.
- ¹⁸Kuzian, R. O., J. Richter, M. D. Kuz'min, and R. Hayn (2016), Physical Review B **93** (21), 214433.
- ¹⁹Lee, H.-J., S.-Y. Jeong, C. R. Cho, and C. H. Park (2002), Applied Physics Letters **81** (21), 4020.
- ²⁰Lee, T. I., S. H. Lee, Y.-D. Kim, W. S. Jang, J. Y. Oh, H. Baik Koo, C. Stampfl, A. Soon, and J. M. Myoung (2012), Nano Letters **12** (1), 68.
- ²¹Martin-Gonzalez, M. S., M. a. Garcia, I. Lorite, J. L. Costa-Kramer, F. Rubio-Marcos, N. Carmona, and J. F. Fernandez (2010), Journal of The Electrochemical Society **157**, E31.
- ²²Martin-Gonzalez, M. S., M. a. Garcia, I. Lorite, J. L. Costa-Kramer, F. Rubio-Marcos, N. Carmona, and J. F. Fernandez (2010), Journal of The Electrochemical Society **157**, E31.
- ²³Matsukura, F., H. Ohno, A. Shen, and Y. Sugawara (1998), Physical Review B **57** (4), R2037.
- ²⁴Mehl, S., P. Ferstl, M. Schuler, A. Toghan, O. Brummel, L. Hammer, M. A. Schneider, and J. Libuda (2015), Phys. Chem. Chem. Phys. **17** (36), 23538.
- ²⁵Methfessel, M., and A. T. Paxton (1989), Phys. Rev. B **40** (6), 3616.
- ²⁶Miller, D. R., S. A. Akbar, and P. A. Morris (2014), Sensors and Actuators B: Chemical **204**, 250.
- ²⁷Montoya, A., and B. S. Haynes (2011), Chemical Physics Letters **502** (1-3), 63.
- ²⁸Netzer, F. P., and A. Fortunelli, Eds. (2016), *Oxide Materials at the Two- Dimensional Limit (Springer Series in Materials Science 234)* (Springer International Publishing).
- ²⁹Noh, J., O. I. Osman, S. G. Aziz, P. Winget, and J.-L. Brédas (2015), Chemistry of Materials **27** (17), 5856.

- ³⁰Olejník, K., M. H. S. Owen, V. Novák, J. Mašek, A. C. Irvine, J. Wunderlich, and T. Jungwirth (2008), *Physical Review B* **78** (5), 054403.
- ³¹Pack, J. D., and H. J. Monkhorst (1977), *Phys. Rev. B* **16** (4), 1748.
- ³²Park, S., S. Kim, H. Kheel, and C. Lee (2015), *Sensors and Actuators, B: Chemical* **222**, 1193.
- ³³Perdew, J. P., K. Burke, and M. Ernzerhof (1996), *Phys. Rev. Lett.* **77** (18), 3865.
- ³⁴Petitto, S. C., and M. A. Langell (2004), *Journal of Vacuum Science & Technology A* **22** (4), 1690.
- ³⁵Quesada, A., M. A. García, M. Andrés, A. Hernando, J. F. Fernández, A. C. Caballero, M. S. Martín-González, and F. Briones (2006), *Journal of Applied Physics* **100** (11), 1.
- ³⁶Rodríguez Torres, C. E., F. Golmar, M. Ziese, P. Esquinazi, and S. P. Heluani (2011), *Phys. Rev. B* **84** (6), 64404.
- ³⁷Roth, W. (1964), *Journal of Physics and Chemistry of Solids* **25** (1), 1.
- ³⁸Sati, P., R. Hayn, R. Kuzian, S. Régnier, S. Schäfer, A. Stepanov, C. Morhain, C. Deparis, M. Laügt, M. Goiran, and Z. Golacki (2006), *Physical Review Letters* **96** (1), 017203.
- ³⁹Sato, K., and H. Katayama-Yoshida (2001), *Japanese Journal of Applied Physics* **40** (4A), L334.
- ⁴⁰Selcuk, S., and A. Selloni (2015), *The Journal of Physical Chemistry C* **119** (18), 9973.
- ⁴¹Sharma, Y., N. Sharma, G. V. Subba Rao, and B. V. R. Chowdari (2007), *Advanced Functional Materials* **17** (15), 2855.
- ⁴²Stefanowicz, S., G. Kunert, C. Simserides, J. A. Majewski, W. Stefanowicz, C. Kruse, S. Figge, T. Li, R. Jakiela, K. N. Trohidou, A. Bonanni, D. Hommel, M. Sawicki, and T. Dietl (2013), *Physical Review B* **88** (8), 081201.
- ⁴³Su, D., S. Dou, and G. Wang (2014), *Scientific reports* **4**, 5767.
- ⁴⁴Thurian, P., G. Kaczmarczyk, H. Siegle, R. Heitz, A. Hoffmann, I. Broser, B. Meyer, R. Hoffbauer, and U. Scherz (1995), *Materials Science Forum* **196-201**, 1571.
- ⁴⁵Vaz, C., V. Henrich, C. Ahn, and E. Altman (2009), *Journal of Crystal Growth* **311** (9), 2648.
- ⁴⁶Walsh, A., S.-H. Wei, Y. Yan, M. M. Al-Jassim, J. A. Turner, M. Woodhouse, and B. A. Parkinson (2007), *Phys. Rev. B* **76** (16), 165119.
- ⁴⁷Wang, M., and Q. Chen (2010), *Chemistry A European Journal* **16** (40), 12088.

- ⁴⁸Wang, X., J. Xu, X. Yu, K. Xue, J. Yu, and X. Zhao (2007), Applied Physics Letters **91** (3), 031908, <http://dx.doi.org/10.1063/1.2759272>.
- ⁴⁹Xu, X.-L., Z.-H. Chen, Y. Li, W.-K. Chen, and J.-Q. Li (2009), Surface Science **603** (4), 653.
- ⁵⁰Xu, X.-L., Z.-H. Chen, Y. Li, W.-K. Chen, and J.-Q. Li (2009), Surface Science **603** (4), 653.
- ⁵¹Zasada, F., W. Piskorz, and Z. Sojka (2015), The Journal of Physical Chemistry C **119** (33), 19180.